Friction
https://doi.org/10.1007/s40544-023-0840-9
ISSN 2223-7690
CN 10-1237/TH
RESEARCH ARTICLE

Core-rim structured MXene@SiO_2 composites as oil-based additives for enhanced tribological properties

Yuhong CUI[1], Shenghua XUE[1], Tiantian WANG[1], Shujuan LIU[1], Qian YE[1,*], Feng ZHOU[1,2,*], Weimin LIU[1,2]

[1] *State Key Laboratory of Solidification Processing, Center of Advanced Lubrication and Seal Materials, School of Materials Science and Engineering, Northwestern Polytechnical University, Xi'an 710072, China*

[2] *State Key Laboratory of Solid Lubrication, Lanzhou Institute of Chemical Physics, Chinese Academy of Sciences, Lanzhou 730000, China*

Received: 08 August 2023 / Revised: 18 September 2023 / Accepted: 16 October 2023

Abstract: Herein, we have prepared SiO_2 particles uploaded MXene nanosheets via *in-situ* hydrolysis of tetraetholothosilicate. Due to the large number of groups at the edges of MXene, SiO_2 grows at the edges first, forming MXene@SiO_2 composites with a unique core-rim structure. The tribological properties of MXene@SiO_2 as lubricating additive in 500 SN are evaluated by SRV-5. The results show that MXene@SiO_2 can reduce the friction coefficient of 500 SN from 0.572 to 0.108, the wear volume is reduced by 73.7%, and the load capacity is increased to 800 N. The superior lubricity of MXene@SiO_2 is attributed to the synergistic effect of MXene and SiO_2. The rolling friction caused by SiO_2 not only improves the bearing capacity but also increases the interlayer distance of MXene, avoiding accumulation and making it more prone to interlayer slip. MXene@SiO_2 is adsorbed on the friction interface to form a physical adsorption film and isolate the friction pair. In addition, the high temperature and high load induce the tribochemical reaction and form a chemical protection film during in the friction process. Ultimately, the presence of these protective films results in MXene@SiO_2 having good lubricating properties.

Keywords: $Ti_3C_2T_x$ MXene; SiO_2 nanoparticles; lubricating additives; protective film

1 Introduction

Friction, as one of the most common phenomena, often occurs on the surfaces of two objects with relative motion. Although friction plays a positive role in situations such as vehicle movement and human walking, the energy loss caused by friction is inevitable [1–3]. According to statistics, energy losses caused by friction and wear account for about one-third of global energy consumption [4]. To solve this problem, the liquid lubricants have been applied to various mechanical equipment to reduce direct contact between solids, resulting in low friction and low wear [5]. However, the performance of traditional base oils has always been limited, resulting in poor lubrication performance and low film forming ability [6, 7]. The use of different nano-additives can improve the lubrication effect and carrying capacity of the base oil [8]. Therefore, it is particularly important to develop a series of efficient and green oil-based lubricating additives.

Over the past two decades, various two-dimensional (2D) materials have been used in tribological research, including MoS_2 [9], black phosphorus [10], and graphene and its derivatives [11, 12], etc. Since Gogotsi et al. found MXene in 2011, the family of 2D nanomaterials has been significantly expanded, and broken new ground in tribology [13]. The chemical formula of MXene is $M_{n+1}X_nT_x$ (n = 1, 2, 3, 4), where M represents the transition metal (Ti, Nb, Mo, etc.), X represents the C or N element, and T_x represents the end functional group [14–17]. The excellent tribological

* Corresponding authors: Qian YE, E-mail: yeqian213@nwpu.edu.cn; Feng ZHOU, E-mail: zhouf@licp.cas.cn

properties of MXene can be traced to their unique layered structure with weak van der Waals forces between layers, which provide a fairly low shear strength for layering [18, 19]. In addition, 2D MXene is prone to adhesion to different surfaces, passivating the contact points and forming a beneficial protective film. However, the most common drawback of 2D MXene as lubricating materials is their inability to work under high contact pressure and sliding speed [20, 21]. In addition, when MXene is used as a lubricating additive in base oil, the hydrophilic groups on the polar surface limit their dispersion stability and cause aggregation in non-polar media. Fortunately, the lipophilicity can be adjusted by functionalization and recombination through the rich functional groups on the surface of MXene [22]. For example, Guo et al. [23] used poly [2-(Perfluorooctyl) ethyl methacrylate)] to modify the MXene and as a lubricant additive, the fluorinated MXene significantly improved the friction reduction and wear resistance of perfluoropolyether. Zhou et al. [24] successfully prepared MXene/HS composites with self-dispersion ability in polyalphaolefin (PAO) 10 through hydrothermal reaction. The ideal combination of MXene and HS produced synergistic lubrication effects through physical interactions and tribochemical reactions.

In addition to 2D materials, spherical nanoparticles are also widely used as high-performance additives, such as copper nanoparticles [25], liquid metals [26], carbon nanospheres [27], etc. SiO_2 is a lubricating material with excellent mechanical properties due to its high hardness and thermal stability. The approximately spherical SiO_2 can be used as a rolling bearing to roll into the high-pressure contact area of the friction pair, thereby improving the extreme pressure characteristics of the lubricating oil. In addition, the surface of nano SiO_2 particles contains a large amount of hydroxyl groups and unsaturated residual bonds, which can form a solid adsorption film on the surface of the friction pair, significantly improving the anti-friction and anti-wear performance of the lubricating oil [28, 29]. For example, Peng et al. [30] studied the effect of different sizes of SiO_2 on the tribological properties of liquid paraffin. It was found that the smaller the size, the greater the load-bearing capacity and wear resistance of liquid paraffin. Razavi et al. [31] found that adding SiO_2 nanoparticles to lithium-based lubricating grease can increase the stiffness of the oil film, reduce direct contact of the friction surface, and improve the tribological and rheological properties of lubricating grease.

In this work, a novel layered MXene@SiO_2 nanocomposite was prepared by *in-situ* growing SiO_2 nanoparticles on MXene nanosheets through controlled hydrolysis of tetraethylorthosilicate (TEOS). Due to the large number of functional groups at the edge of MXene, SiO_2 first grew at the edge of MXene to maintain structural stability, forming a unique non-uniform core-rim structure. The structure evolution and tribological properties of MXene@SiO_2 with different SiO_2 loadings in base oil 500 SN were investigated, and the lubrication mechanism was also discussed in-detail.

2 Experimental sections

2.1 Materials

TEOS (>99%) was obtained from Shanghai Aladdin Biochemical Technology Co., Ltd. Hydrochloric acid (HCl) and ethyl alcohol absolute were purchased from Sinopharm Chemical Reagent Beijing Co., Ltd. Lithium fluoride (LiF) and ammonium hydroxide ($NH_3{\cdot}H_2O$) were provided by Energy Chemical. Ti_3AlC_2 MAX came from Jinzhou Haixin Metal Materials Co., Ltd. All reagents are of analytical grade and can be used directly without further purification.

2.2 Fabrication of single layer or few layer MXene nanosheets

Based on our previous work, single-layer or few-layer dispersions of $Ti_3C_2T_x$ MXene nanosheets were prepared [32]. First, 1 g of LiF and 20 mL of HCl (9 M) were magnetically stirred in a reaction vessel of polytetrafluoroethylene for 10 min to form a uniform solution. Then, 1 g of Ti_3AlC_2 MAX powder was slowly added to the mixture and magnetically stirred at 35 °C for 24 h. After the reaction, the mixture was washed by centrifugation using deionized water. First, the solution was washed several times by centrifugation at 4,000 rpm until the upper solution turned black. Then increased the speed to 8,000 rpm, continue

centrifugal washing, and finally increased the speed to 10,000 rpm, continue centrifugal washing until the upper solution turned black and viscous. After centrifugation, the upper layer solution was taken for ultrasonic treatment, and the MXene nanosheets separated from the upper layer were collected by centrifugation.

2.3 Preparation of MXene@SiO_2 composites

SiO_2 nanoparticles were *in-situ* grown on MXene nanosheets by hydrolysis of TEOS [33]. Typically, 10 mL of MXene nanosheet dispersion was added to a mixture of 100 mL ethanol and water (1:1) and stirred for 30 min. Then, 6 mL $NH_3{\cdot}H_2O$ was added into the above solution, and TEOS with different weights were slowly dropped into the solution, and stirred at room temperature for 6 h to obtain MXene@SiO_2 composites with different SiO_2 loadings. After the reaction, in order to remove the residual solvent, the product was centrifuged and washed with deionized water. Finally, MXene@SiO_2 composite materials were collected by freeze-drying method. The products with TEOS additions of 0.2, 0.4, and 0.6 mL were named MXene@SiO_2-1, MXene@SiO_2-2, and MXene@SiO_2-3, respectively.

2.4 Characterization

Morphological characteristics of MXene, MXene@SiO_2-1, MXene@SiO_2-2, and MXene@SiO_2-3 were characterized by transmission electron microscope (TEM, Talos F200X) and scanning electron microscopy (SEM, Tescan Clara GMH). Fourier infrared spectra (FTIR, Bruker, TENSOR II) was used to measure the surface functional groups of different samples. X-ray diffraction (XRD, Thermo Scientific 7000) patterns were conducted in the range of 5°–90°, and the scanning speed was 5°/min. X-ray photoelectron spectroscopy (XPS, PHI 5000 VersaProbe III) were used to analyze the surface chemical state. The full XPS spectrum range was 0–1,100 eV and the step size was 1 eV. For the narrow spectrum, each element was scanned 5 times and cycled twice, and the step size was 0.125 eV. Using three-dimensional (3D) surface profiler to observe the wear status of scratches.

The tribological properties of different additives were studied using a micro-action friction and wear tester (SRV-5). The friction pair consists of a steel ball and a steel disc. The ball (ø 10 mm, hardness: 60 ± 2 HRC, mean roughness: 20 nm) and disc (ø 24 mm × 7.9 mm, hardness: 62 ± 2 HRC) were all made of AISI 52100 steel. Variable load test: under the conditions of amplitude of 1 mm, temperature of 50 °C, and frequency of 25 Hz, the load started at 50 N and increased by 50 N every 5 min. Frequency conversion test: under the condition of amplitude of 1 mm, temperature of 50 °C and load of 150 N. The frequency increased from 5 to 50 Hz, increasing by 5 Hz every 5 min. Variable temperature test: under the condition of amplitude of 1 mm, frequency of 25 Hz and load of 150 N. The temperature rose from 40 to 120 °C, increasing by 10 °C every 5 min.

3 Results and discussion

The preparation process of MXene@SiO_2 composites was shown in Scheme 1. $Ti_3C_2T_x$ MXene nanosheets were obtained by selective removal of the Al atomic layer from Ti_3AlC_2 MAX by *in-situ* formation of HF etching from a mixed HCl–LiF solution. Afterwards, 2D MXene with single or fewer layers can be obtained by ultrasonication. The H, O, and F atoms in the etching medium bond with the surface unsaturated Ti atoms, forming surface end groups such as –OH, –O, or –F on the surface of MXene, resulting in the final formation of MXene materials with mixed groups on the surface. As shown in Figs. 1(a)–1(d), due to the high number of functional groups at the edge of MXene, it provided a large number of nucleation sites for TEOS hydrolysis. Therefore, when a small amount of TEOS was added, SiO_2 preferentially grew at the edge of the MXene layer, forming a unique core-rim structure. As TEOS increased, SiO_2 gradually diffused from the edge of the MXene to the surface.

The morphologies of different samples were observed by SEM and TEM. The original precursor of Ti_3AlC_2 MAX was an irregularly layered bulk material (Fig. S1 in the Electronic Supplementary Material (ESM)) [34]. MXene nanosheets were obtained by sonication after removing the Al layer with HCl–LiF solution (Fig. 1(e)). The TEM image in Fig. 1(i) showed the transparent state of MXene, which indicated that the prepared MXene had a monolayer or few-layer

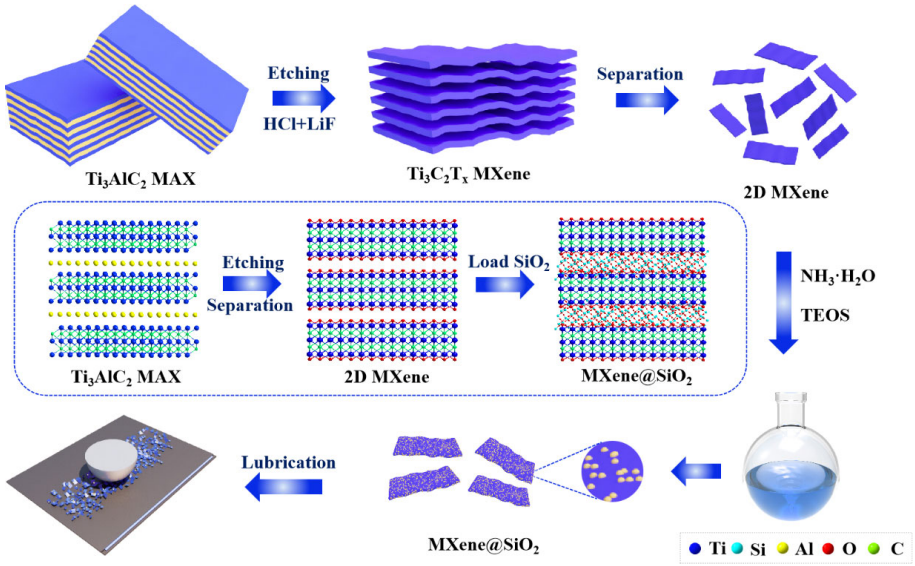

Scheme 1 Schematic diagram of the preparation process of MXene@SiO_2.

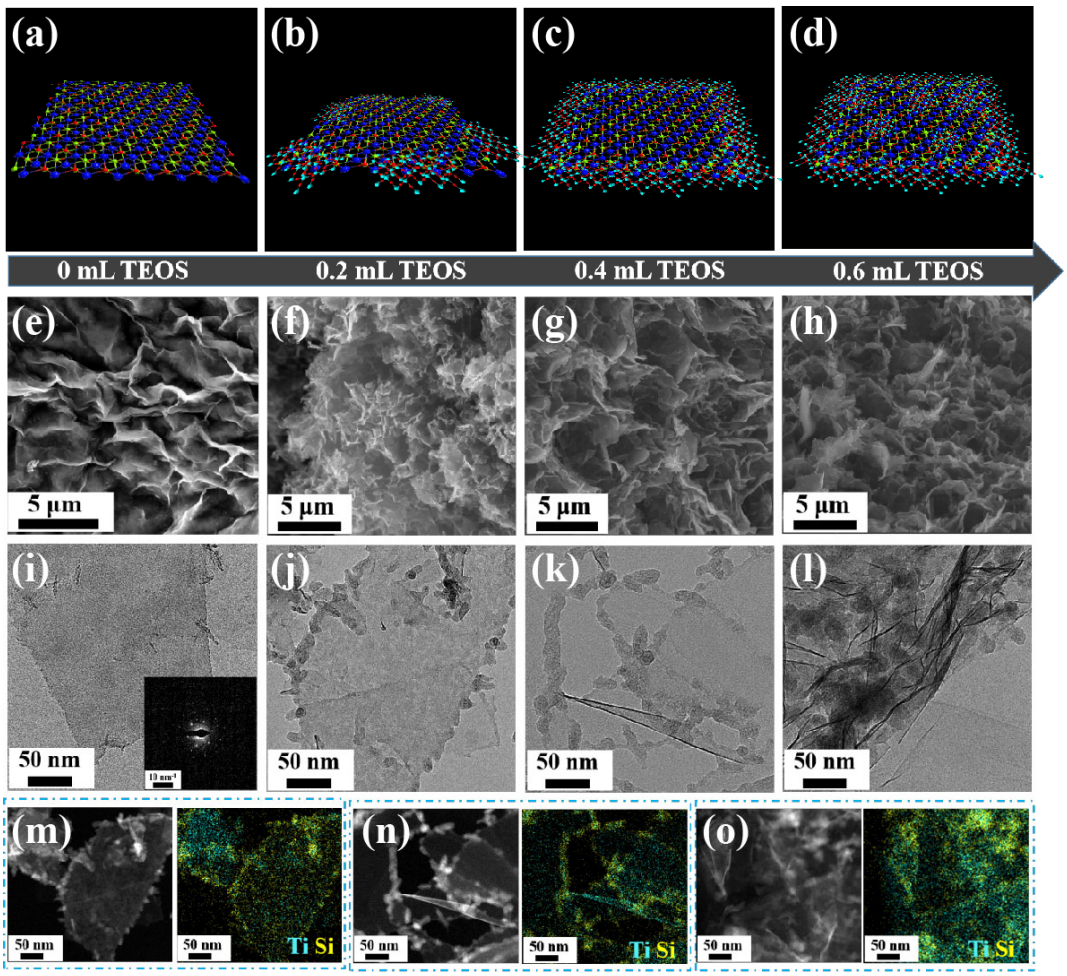

Fig. 1 (a–d) Structural changes of MXene@SiO_2 with different levels of TEOS. SEM and TEM images of (e, i) MXene, (f, j) MXene@SiO_2-1, (g, k) MXene@SiO_2-2, and (h, l) MXene@SiO_2-3. High angle annular dark field (HAADF) images and element mapping analysis of Ti and Si of (m) MXene@SiO_2-1, (n) MXene@SiO_2-2, and (o) MXene@SiO_2-3.

structure. The hexagonal crystal structure of MXene was confirmed by selected area electron diffraction [35]. Figures 1(f)–1(h) showed the SEM images of MXene@SiO_2-1, MXene@SiO_2-2, and MXene@SiO_2-3 at TEOS addition amounts of 0.2, 0.4, and 0.6 mL. It can be seen that all samples maintained a lamellar structure. As can be seen from the TEM images, the edges of MXene@SiO_2-1 and MXene@SiO_2-2 were covered with particles and became rough when a small amount of TEOS was added, which indicated that SiO_2 nanoparticles first grew at the edge of the MXene nanosheets (Figs. 1(j) and 1(k)). The elemental mapping analysis in Fig. S2 in the ESM determined the elemental composition of MXene@SiO_2, including Si, Ti, O, and C elements. Meanwhile, the Ti element was surrounded by Si element, which proved its unique core-rim structure (Figs. 1(m) and 1(n)). Compared with MXene@SiO_2-1 and MXene@SiO_2-2, the SiO_2 nanoparticles in MXene@SiO_2-3 were uniformly distributed on the edge and surface of the MXene and their sizes gradually increased.

The surface functional groups of MXene, MXene@SiO_2-1, MXene@SiO_2-2, and MXene@SiO_2-3 were measured by FTIR spectroscopy, and the results were shown in Fig. 2(a). All samples showed a peak near 3,451.4 cm^{-1} corresponding to the stretching vibration of –OH. The peaks at 1,626.2 and 561.2 cm^{-1} were due to C=C and Ti–O bonds, respectively. In addition, the peaks of MXene@SiO_2 at 1,089.4 and 466.7 cm^{-1} were caused by asymmetric or bending vibrations of Si–O–Si and tensile vibrations of Si–O [36, 37]. As the loading amount of SiO_2 increased, the peak value of Si–O and Si–O–Si bonds became larger and larger. Figure 2(b) showed the XRD patterns of the different samples, from which it can be seen that all the samples had a distinct characteristic peak below 10°, corresponding to the (002) crystal plane of MXene. After loading SiO_2, the position of the (002) peak was gradually shifted to a smaller angle, which was manifested as an increase in the interlayer spacing [38]. The surface chemical states of the MXene@SiO_2 composites were further explored by XPS spectroscopy. As shown in Fig. 2(c), the XPS full spectra of MXene@SiO_2-1, MXene@SiO_2-2, and MXene@SiO_2-3 showed the appearance of additional Si 2p peaks compared to MXene, which indicated the successful complexation of MXene with SiO_2. In Figs. 2(d) and 2(e), the gray line with circle icon represented the raw measured data, the red line represented the peak fitted data, and the areas filled with different colors

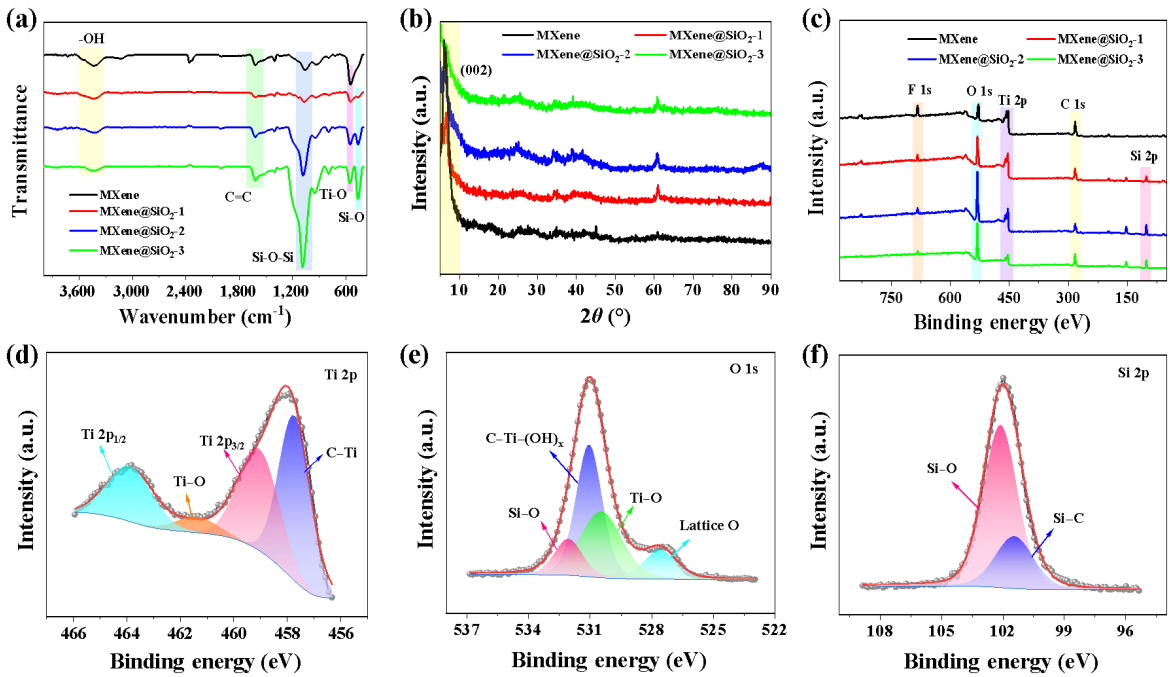

Fig. 2 (a) FTIR spectra, (b) XRD patterns, and (c) XPS full spectra of MXene, MXene@SiO_2-1, MXene@SiO_2-2, and MXene@SiO_2-3. High-resolution XPS spectra of MXene@SiO_2-2: (d) Ti 2p, (e) O 1s, and (f) Si 2p.

represented different peak information. The high-resolution Ti 2p spectrum of MXene@SiO_2-2 can accumulate five characteristic peaks corresponding to C–Ti (457.8 eV), Ti $2p_{3/2}$ (459.1 eV), Ti–O (461.5 eV), and Ti $2p_{1/2}$ (463.9 eV) (Fig. 2(d)). In the O 1s spectrum, the peaks located at 527.6, 530.5, 531.3, and 532.1 eV were caused by lattice O, Ti–O, C–Ti–$(OH)_x$, and Si–O, respectively (Fig. 2(e)). The peaks at 101.5 and 102.1 eV in the high-resolution Si 2p spectrum were attributed to Si–C and Si–O (Fig. 2(f)). As shown in Fig. S3 in the ESM, the peak of C 1 s spectrum consisted of C–Ti (281.9 eV), C–C (284.6 eV), C–OH (286.1 eV), and C=O bonds (288.4 eV) [39, 40].

As shown in Fig. S4 in the ESM, the dispersion stability of MXene, MXene@SiO_2-1, MXene@SiO_2-2, and MXene@SiO_2-3 in 500 SN were investigated. First, $Ti_3C_2T_x$ MXene, MXene@SiO_2-1, MXene@ SiO_2-2, and MXene@SiO_2-3 were fully dispersed in the base oil 500 SN through ultrasonic treatment to obtain a stable black mixture, and the concentration of all mixtures was 2.4 wt%. After that, the samples were left to stand to observe the precipitation state. From Fig. S4 in the ESM, we can see that after ultrasonic treatment, all additives can be dispersed in 500 SN to form a uniform mixture. When the samples were left for five days, the color of the upper solution became lighter, indicating that all samples had a small amount of precipitation. After eight days, the upper solution in 500 SN containing MXene turned yellow and a large amount of precipitation appeared, which was due to the large number of hydrophilic groups on the surface of MXene. Compared with MXene@SiO_2-1 and MXene@SiO_2-2, 500 SN containing MXene@SiO_2-3 had more precipitation. This showed that excessive SiO_2 will increase the weight of MXene nanosheets, and appropriate SiO_2 will occupy part of the hydrophilic groups on the surface of MXene, resulting in an increase in lipophilicity.

The coefficient of friction (COF) and wear volume were used to evaluate the anti-friction and anti-wear performance of different samples. The COF curves of all samples over time were measured using SRV-5, and the results were shown in Fig. 3. The concentration of additives significantly affected the lubrication performance of lubricating oil. Therefore, we measured the COF of MXene@SiO_2-2 at 150 N, 25 Hz, and 50 °C in the concentration range of 1.2 wt%–2.8 wt%. As shown in Fig. 3(a), when the concentration was too low or high, the COF stabilized and tended to a straight line at the beginning of the friction, whereas the COF gradually rose in the later part of the run, and the average COF reached the lowest value at 2.4 wt% (Fig. S5 in the ESM). This was because when the concentration was too low, a continuous and stable protective film cannot be formed, while when the concentration was too high, excessive sample deposition prevented the formation of a friction film and increased wear on the contact surfaces [41, 42]. To further compare the tribological properties of MXene, MXene@SiO_2-1, MXene@SiO_2-2, and MXene@SiO_2-3, the COF versus over time were measured at a concentration of 2.4 wt% (Fig. 3(b)). The COF of the base oil 500 SN sharply increased within 100 s, generated a large friction noise and seizing failure occurred. At the same time, the stroke of the steel ball on the steel plate increased sharply, and after reaching stability, the stroke remained at 1 mm (Fig. S6 in the ESM). The COF curves of MXene and MXene@SiO_2-1 were similar, with a sudden surge at the end of preloading, but compared to 500 SN, the average COF decreased from 0.180 to 0.140 and 0.141. This was because when the amount of TEOS added was relatively small, only a small amount of SiO_2 nanoparticles were present at the edge of MXene. Although it improved the lipophilicity of MXene to some extent, due to its small size and insufficient quantity, MXene still exhibited partial stacking phenomenon. In contrast, MXene@SiO_2-2 showed good friction reduction performance, not only avoiding friction peaks, but also maintaining a stable COF during operation, with an average COF of 0.108. The addition of MXene@SiO_2-3 also avoided the initial friction peak, but the average COF rose to 0.127 compared to MXene@SiO_2-2. This implied that too little or too much SiO_2 is not conducive to improving lubrication performance (Fig. 3(c)).

Figures 3(d)–3(f) compared the lubrication performance of different samples under extreme conditions. Figure 3(d) showed lubrication failure of base oil 500 SN at 100 N. The addition of MXene and MXene@SiO_2-1 can increase the carrying capacity of 500 SN to 200 N. This indicated that when there were

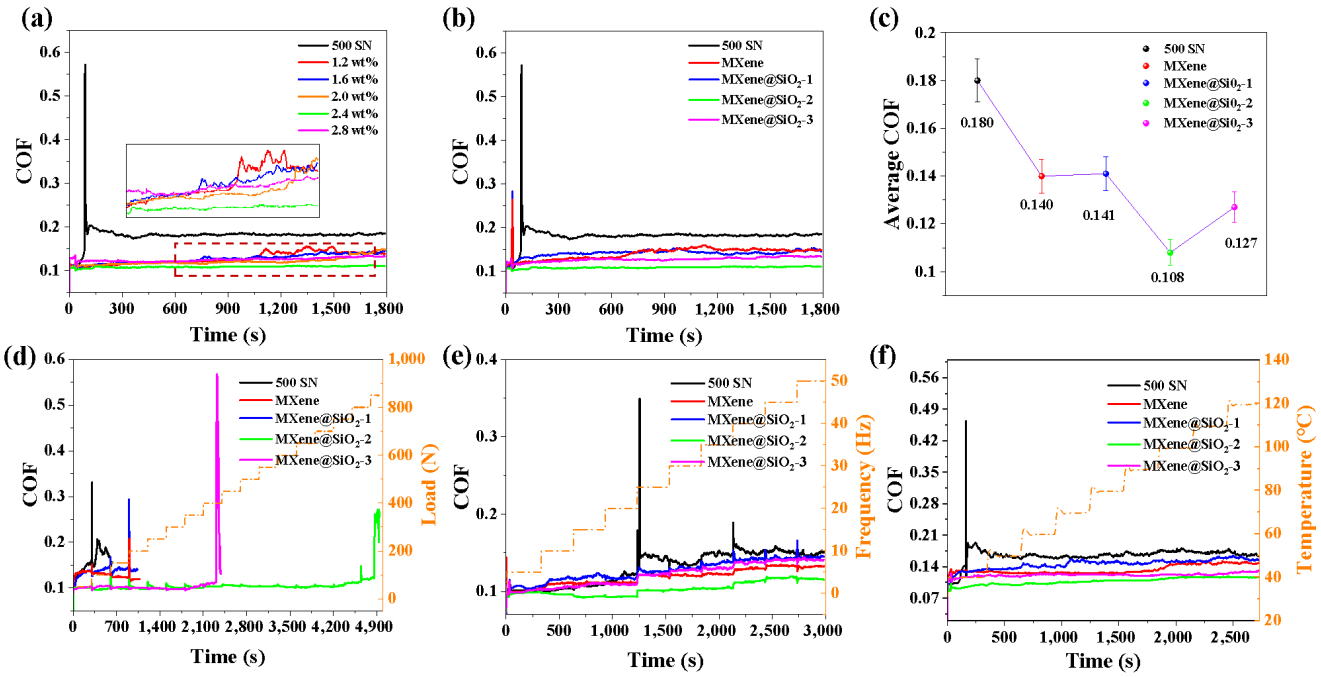

Fig. 3 (a) COF curves of MXene@SiO_2-2 at different concentrations. (b) COF curves and (c) average COF of 500 SN, MXene, MXene@SiO_2-1, MXene@SiO_2-2, and MXene@SiO_2-3 (2.4 wt%). COF curves of all additives with the change of (d) load, (e) frequency, and (f) temperature.

fewer SiO_2 particles, it was difficult to form a friction film that supported the load, so the load resistance will not be significantly improved. The load carrying capacity of 500 SN reached 800 N with the addition of MXene@SiO_2-2. While with the addition of MXene@SiO_2-3, the load carrying capacity dropped to 400 N. This indicated that appropriate SiO_2 can serve as a rolling bearing to form a protective film that can support the load to compensate for the low loading capacity of MXene. When SiO_2 was excessive or large in size, it was not conducive to continuous entry into the contact area of the friction pair, resulting in a decrease in load carrying capacity. In different frequency and temperature tests, MXene@SiO_2-2 also exhibited the best tribological performance, with the lowest COF and maintaining stability (Figs. 3(e) and 3(f)). This showed that MXene@SiO_2-2 can adapt to heavy-duty, high-speed, and high-temperature operating conditions and maintain excellent lubrication performance.

In order to further evaluate the wear resistance of different samples, the wear scratches on the lower disk of the friction pair were characterized by 3D profilometer and SEM. Consistent with the results of friction reduction, at a concentration of 2.4 wt%, the wear depth and wear volume of MXene@SiO_2-2 were the smallest (Figs. S7–S9 in the ESM). Figure 4 compared the morphology of wear and scratch marks after lubricated by 500 SN, MXene, MXene@SiO_2-1, MXene@SiO_2-2, and MXene@SiO_2-3. The wear scratches after lubricated by 500 SN showed wide and deep grooves, and the maximum wear depth was 2.357 μm. The corresponding SEM images clearly showed a large number of grooves and uneven particles on the worn surface. These uneven particles further accelerated the wear of the interface (Figs. 4(a1)–4(a4)). As shown in Figs. 4(b1)–4(b4), after adding MXene to 500 SN, the wear depth decreased to 2.095 μm. However, SEM images showed that there were still quite a few grooves on the surface. The addition of MXene@SiO_2-1 slightly increased the wear depth, but the grooves on the wear surface became shallower (Figs. 4(c1)–4(c4)). Compared with 500 SN, the addition of MXene@SiO_2-2 resulted in a significant reduction in the wear width and wear depth, with the maximum wear depth decreasing to 1.098 μm, while the wear surface became relatively smooth, with very few and shallow grooves appearing (Figs. 4(d1)–4(d4)). After

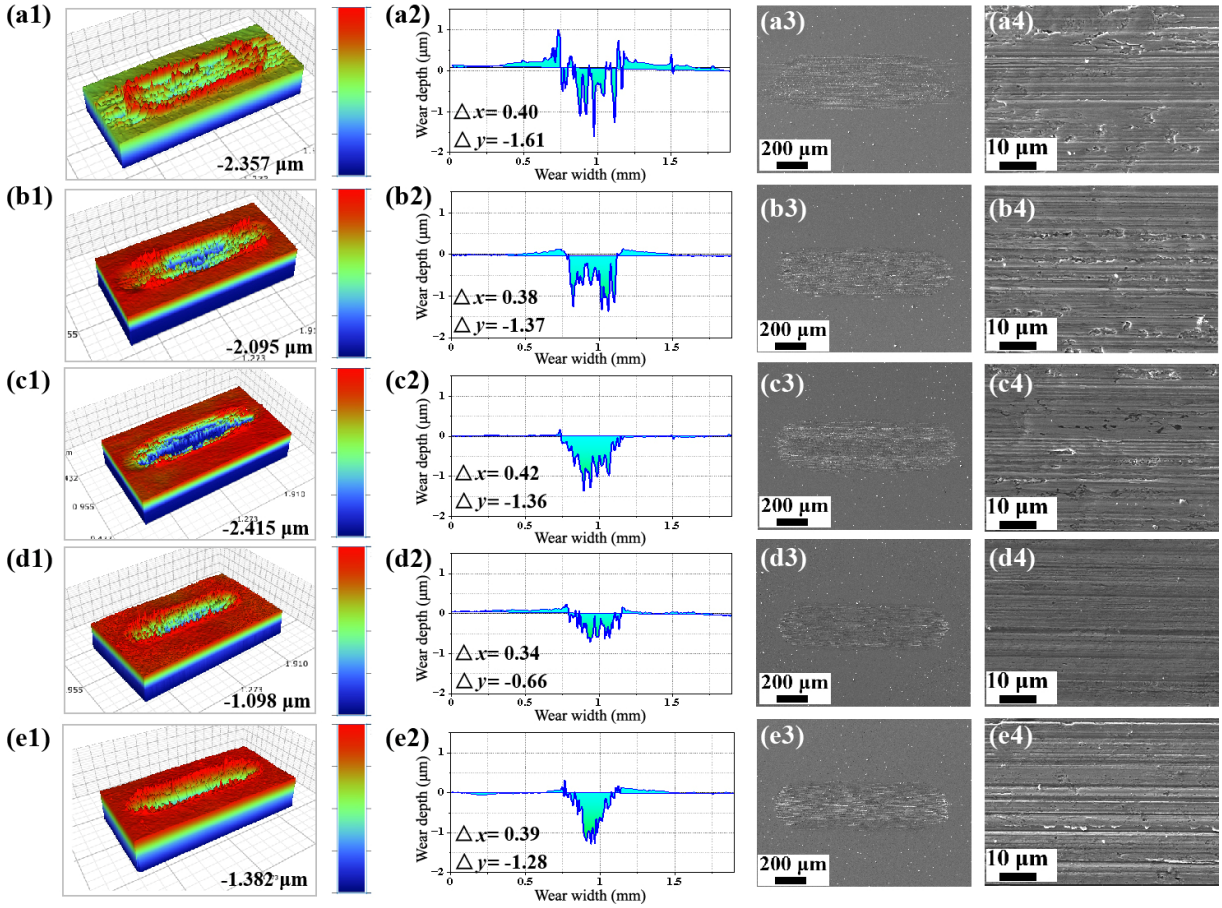

Fig. 4 3D images, wear depth, and SEM images on the wear scar of the disk lubricated by (a1–a4) 500 SN, (b1–b4) MXene, (c1–c4) MXene@SiO_2-1, (d1–d4) MXene@SiO_2-2, and (e1–e4) MXene@SiO_2-3.

adding MXene@SiO_2-3, the maximum wear depth decreased to 1.382 μm and grooves still appeared on the wear surface (Figs. 4(e1)–4(e4)). In addition, the element mapping analysis of the worn surface after MXene@SiO_2-2 lubrication was shown in Fig. S10 in the ESM. C, Ti, Si, O, and Fe elements were uniformly distributed on the worn surface. This indicated that appropriate interaction between SiO_2 and MXene can easily form a friction film on the contact surface of steel, promoting sliding by reducing friction, thereby reducing wear trajectory [43].

The wear volume of the lower disk of the friction pair after lubrication of different samples was shown in Fig. 5(a). The wear volume after base oil lubrication was as high as 5.36×10^5 μm^3. With the addition of MXene, the wear volume dropped to 3.01×10^5 μm^3, reduced by 43.8%. When loading a small or excessive amount of SiO_2, the wear volume after MXene@SiO_2-1 and MXene@SiO_2-3 lubrication was decreased by 44.7% and 57.1%. Loading appropriate SiO_2 can significantly improve the wear resistance of the sample. Compared with 500 SN, after adding MXene@SiO_2-2, the wear volume decreased to 1.41×10^5 μm^3, reduced by 73.7%. Figure 5(b) summarized the friction reduction and anti-wear properties of all the samples, and MXene@SiO_2-2 outperformed the other samples in all the evaluated metrics (average COF, loading capacity, wear volume, and wear depth), reflecting the superiority of its tribological properties.

XPS spectra of wear surface after MXene@SiO_2-2 lubrication was investigated to further analyze the chemical composition of the friction protection film and the lubrication process. The full XPS spectrum of Fig. 6(a) showed not only major Fe and O elements, but also the presence of Ti, C, and Si elements, which was consistent with the results of elemental mapping analysis in Fig. S10 in the ESM. As shown in Fig. 6(b), two characteristic peaks of Fe_3O_4 and Fe_2O_3 can be

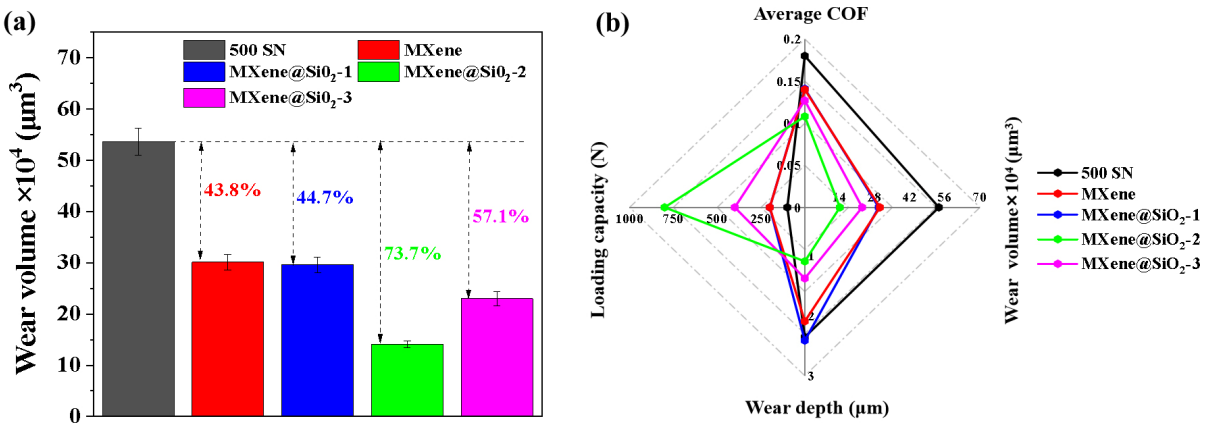

Fig. 5 (a) Wear volume of wear scar on lower disk lubricated by 500 SN, MXene, MXene@SiO_2-1, MXene@SiO_2-2, and MXene@SiO_2-3. (b) Comparison of tribological properties of different samples.

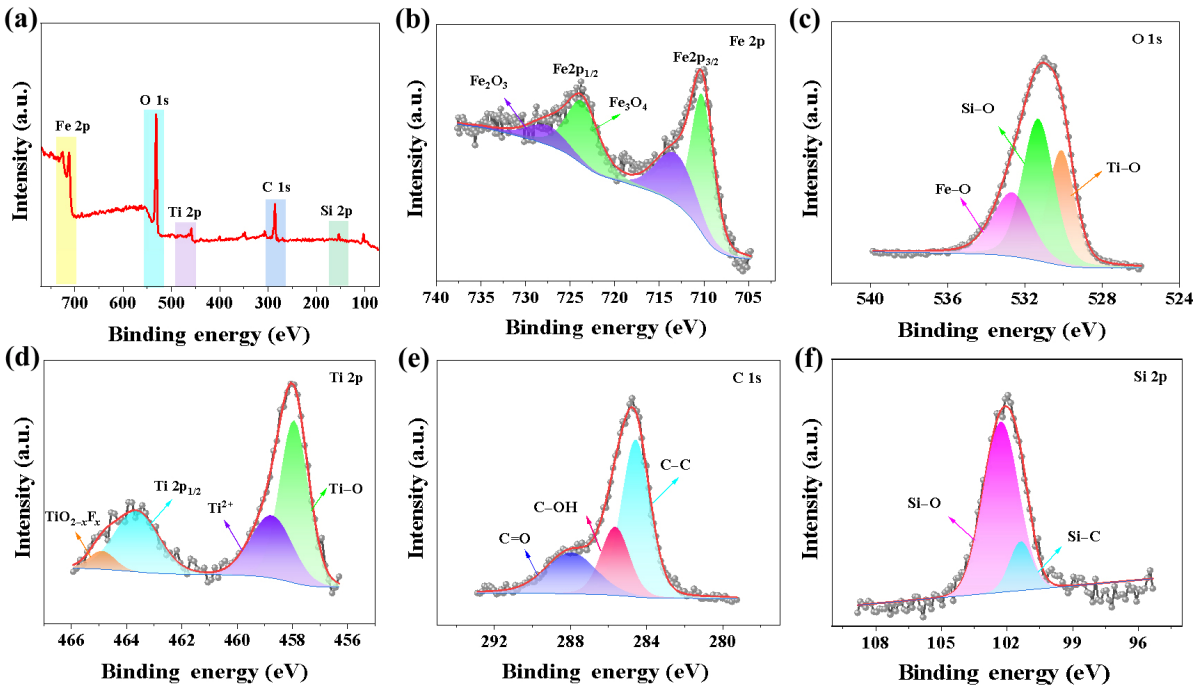

Fig. 6 (a) XPS full spectrum and high-resolution XPS spectra of (b) Fe 2p, (c) O 1s, (d) Ti 2p, (e) C 1s, and (f) Si 2p on the wear scar of the disk.

fitted in the Fe 2p peak, which indicated that part of the Fe element was oxidized during the friction process. In the O 1s spectrum, the peaks located at 530.2, 531.9, and 532.6 eV were attributed to Ti–O, Si–O, and Fe–O bonds, respectively. The Fe–O bond corresponded to the oxide of Fe in Fe 2p, and the Ti–O and Si–O peaks originated from MXene and SiO_2, respectively (Fig. 6(c)). The XPS spectrum of Ti 2p in Fig. 6(d) consisted of four characteristic peaks, corresponding to Ti–O (457.9 eV), Ti^{2+} (458.8 eV), Ti $2p_{1/2}$ (463.7 eV), and $TiO_{2-x}F_x$ (464.9 eV), respectively. The C1s peak was composed of C–C, C–OH, and C=O bonds (Fig. 6(e)). The peaks of Si 2p at 101.4 and 102.2 eV were caused by Si–C and Si–O (Fig. 6(f)) [43, 44]. Therefore, it can be inferred from the above XPS analysis that MXene@SiO_2 can be deposited on the wear surface to form a physical adsorbed film. Due to the high load and high temperature at the sliding interface, MXene@SiO_2 induced frictional chemical reaction, forming a chemical protective film mainly composed of TiO_2, Fe_2O_3, and Fe_3O_4. The physical and chemical film adsorbed on the worn surface and

played an effective protective role on the friction interface [45].

The lubrication mechanism of MXene@SiO_2 as an additive in 500 SN was shown in Scheme 2. Because SiO_2 improved the lipophilicity of MXene, MXene@SiO_2 had good dispersion stability in the base oil 500 SN. Therefore, in the process of friction, MXene@SiO_2 can enter the contact area of the friction pair with the flow of the base oil and adsorbed on the wear surface. Under the bidirectional action of pressure and shear force, SiO_2 widened the interlayer distance between MXene nanosheets, making it more prone to interlayer slip and fully utilizing the interlayer shear mechanism. SiO_2 with high hardness and thermal stability can be rolled into the high-pressure contact area as a rolling bearing to enhance bearing capacity. In addition, MXene@SiO_2 broke into smaller fragments to fill in the pits and valleys of the friction vice, smoothing the contact surface and acting as a repair. In the rapid reciprocating operation during friction, the high temperature and high load induced friction chemical reaction to occur, forming a chemical reaction film dominated by Fe oxide and Ti oxide to improve the interaction at the interface. In summary, the good lubricating properties of MXene@SiO_2 were attributed to the effect of synergistic lubrication.

4 Conclusions

In this work, SiO_2 modified MXene nanocomposite materials were synthesized via a simple self-growth method. The growth position of SiO_2 can be controlled by controlling the addition of tetraethylorthosilicate (TEOS), resulting in the formation of MXene@SiO_2 composites with a unique non-uniform core-rim structure. The prepared MXene@SiO_2 had good dispersion stability in base oil 500 SN and thus exhibited excellent tribological properties. When added at a concentration of 2.4 wt%, the coefficient of friction (COF) of 500 SN reduced from 0.572 to 0.108, the wear volume decreased from 5.36×10^5 to 1.41×10^5 μm^3, and the load capacity increased to 800 N. Its excellent tribological properties were due to the synergistic effect of MXene and SiO_2. The laminar structure of MXene facilitated interlayer slip during friction, and the spherical structure of SiO_2 can be used as a rolling bearing to enhance the load carrying capacity. In addition, the good dispersion stability of MXene@SiO_2 ensured a continuous supply of samples to form a stable and continuous protection film to isolate the contact surface of the friction partner. This study enriched the application of MXene-based nanocomposites as lubrication additives and had great potential in mechanical lubrication system.

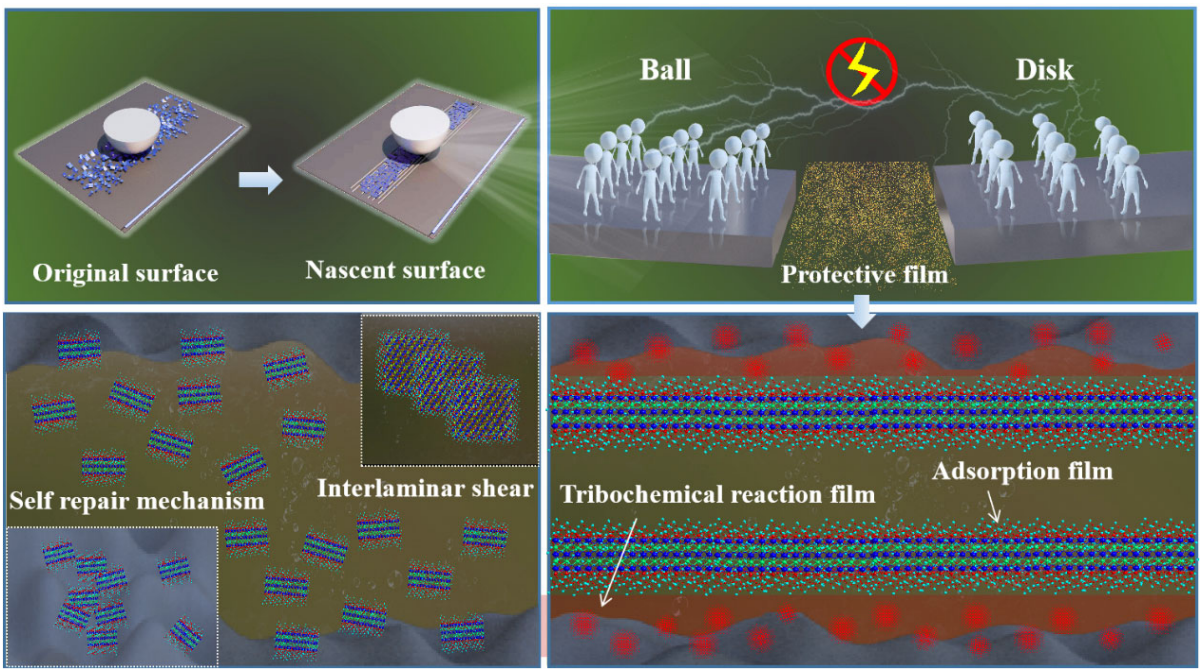

Scheme 2 Anti-friction and anti-wear mechanism of MXene@SiO_2 composites.

Acknowledgements

This work was supported by the National Natural Science Foundation of China (51972272, U21A2046), the Western Light Project of CAS (xbzg-zdsys-202118), and the Research Fund of the State Key Laboratory of Solidification Processing (NPU), China (2023-TS-03).

Declaration of competing interest

The authors have no competing interests to declare that are relevant to the content of this article. The authors Feng ZHOU and Weimin LIU are the Editorial Board Members of this journal.

Electronic Supplementary Material: Supplementary material is available in the online version of this article at https://doi.org/10.1007/s40544-023-0840-9.

References

[1] Zhang X Z, Lu Q, Yan Y J, Zhang T T, Liu S J, Cai M R, Ye Q, Zhou F, Liu W M. Tribochemical synthesis of functionalized covalent organic frameworks for anti-wear and friction reduction. *Friction* **11**(10): 1804–1814 (2023)

[2] Yan Y J, Zhang X Z, Cui Y H, Xue S H, Liu S J, Ye Q, Zhou F. Fabrication of ionic liquid-functionalized covalent organic frameworks for friction and wear reduction. *J Mol Liq* **382**: 122026 (2023)

[3] Wang Y X, Xue S H, Liu S, Xu F, Liu S J, Ye Q, Zhou F, Liu W M. Polystyrene-derived porous graphite carbon nanospheres with corrosion resistance as a lubricant additive for efficient friction and wear reduction. *Tribol Int* **189**: 108957 (2023)

[4] Cui Y H, He B L, Xue S H, Chen Z, Liu S J, Ye Q, Zhou F, Liu W M. Fabrication of MXene@Fe_3O_4@PNA composite with photothermal effect as water-based lubricant additive. *Chem Eng J* **469**: 143880 (2023)

[5] Zhai W Z, Zhou K. Nanomaterials in superlubricity. *Adv Funct Materials* **29**(28): 1806395 (2019)

[6] Jin B, Chen G Y, Zhao J, He Y Y, Huang Y Y, Luo J B. Improvement of the lubrication properties of grease with Mn_3O_4/graphene (Mn_3O_4#G) nanocomposite additive. *Friction* **9**(6): 1361–1377 (2021)

[7] Wang T, He B, Xue S, Chen X, Liu S, Ye Q, Zhou F, Liu W M. Supramolecular gelator functionalized liquid metal nanodroplets as lubricant additive for friction reduction and anti-wear. *J Colloid Interf Sci* **653**: 258–266 (2024)

[8] Li X W, Zhang D K, Xu X W, Lee K R. Tailoring the nanostructure of graphene as an oil-based additive: Toward synergistic lubrication with an amorphous carbon film. *ACS Appl Mater Interfaces* **12**(38): 43320–43330 (2020)

[9] Feng P, Ren Y P, Li Y T, He J F, Zhao Z, Ma X L, Fan X Q, Zhu M H. Synergistic lubrication of few-layer $Ti_3C_2T\_x$/MoS_2 heterojunction as a lubricant additive. *Friction* **10**(12): 2018–2032 (2022)

[10] Tang G B, Su F H, Xu X, Chu P K. 2D black phosphorus dotted with silver nanoparticles: An excellent lubricant additive for tribological applications. *Chem Eng J* **392**: 123631 (2020)

[11] Lu Q, Zhang T Y, Wang Y X, Liu S J, Ye Q A, Zhou F. Boron–nitrogen codoped carbon nanosheets as oil-based lubricant additives for antioxidation, antiwear, and friction reduction. *ACS Sustainable Chem Eng* **11**(32): 11867–11877 (2023)

[12] Fan X Q, Li X P, Zhao Z, Yue Z F, Feng P, Ma X L, Li H, Ye X Y, Zhu M H. Heterostructured rGO/MoS_2 nanocomposites toward enhancing lubrication function of industrial gear oils. *Carbon* **191**: 84–97 (2022)

[13] Cai M, Yan H, Song S J, He D M, Lin Q L, Li W, Fan X Q, Zhu M H. State-of-the-art progresses for Ti3C2Tx MXene reinforced polymer composites in corrosion and tribology aspects. *Adv Colloid Interface Sci* **309**: 102790 (2022)

[14] Zeng Y X, Wang P, He B L, Liu S J, Ye Q, Zhou F. Fabrication of zwitterionic polymer-functionalized MXene nanosheets for anti-bacterial and anti-biofouling applications. *Prog Org Coat* **183**: 107727 (2023)

[15] Cui Y H, Yang K, Zhang F R, Lyu Y T, Zhang Q Y,

Zhang B L. Ultra-light MXene/CNTs/PI aerogel with neat arrangement for electromagnetic wave absorption and photothermal conversion. *Compos A* **158**: 106986 (2022)

[16] Qu D Y, Jian Y Y, Guo L H, Su C, Tang N, Zhang X M, Hu W W, Wang Z, Zhao Z H, Zhong P, *et al*. An organic solvent-assisted intercalation and collection (OAIC) for $Ti_3C_2T\_x$ MXene with controllable sizes and improved yield. *Nano Micro Lett* **13**(1): 188 (2021)

[17] Wang P, He B L, Wang B W, Liu S J, Ye Q, Zhou F, Liu W M. MXene/Metal-Organic framework based composite coating with photothermal self-healing performances for antifouling application. *Chem Eng J* **474**: 145835 (2023)

[18] Gao J D, Du C F, Zhang T T, Zhang X Z, Ye Q A, Liu S J, Liu W M. Dialkyl dithiophosphate-functionalized $Ti_3C_2T_x$ MXene nanosheets as effective lubricant additives for antiwear and friction reduction. *ACS Appl Nano Mater* **4**(10): 11080–11087 (2021)

[19] Cai M, Feng P, Yan H, Li Y T, Song S J, Li W, Li H, Fan X Q, Zhu M H. Hierarchical $Ti_3C_2T_x$@MoS_2 heterostructures: A first principles calculation and application in corrosion/wear protection. *J Mater Sci Technol* **116**: 151–160 (2022)

[20] Miao X N, Li Z P, Liu S W, Wang J Q, Yang S R. MXenes in tribology: Current status and perspectives. *Adv Powder Mater* **2**(2): 100092 (2023)

[21] Chen X, Xue S H, Yan Y J, Bai W, Du C F, Liu S J, Ye Q, Zhou F. Zwitterionic polymer-functionalized nitrogen-doped MXene nanosheets as aqueous lubricant additive. *Tribol Int* **186**: 108625 (2023)

[22] Parra-Muñoz N, Soler M, Rosenkranz A. Covalent functionalization of MXenes for tribological purposes—A critical review. *Adv Colloid Interface Sci* **309**: 102792 (2022)

[23] Guo J L, Wu P X, Zeng C, Wu W, Zhao X Y, Liu G Q, Zhou F, Liu W M. Fluoropolymer grafted $Ti_3C_2T_x$ MXene as an efficient lubricant additive for fluorine-containing lubricating oil. *Tribol Int* **170**: 107500 (2022)

[24] Zhou C Z, Li Z P, Liu S W, Ma L M, Zhan T R, Wang J Q. Synthesis of MXene-based self-dispersing additives for enhanced tribological properties. *Tribol Lett* **70**(2): 1–13 (2022)

[25] Xue Y W, Shi X L, Huang Q P, Zhang K P, Wu C H. Effects of groove-textured surfaces with Sn-Ag–Cu and MXene–Ti_3C_2 on tribological performance of CSS-42L bearing steel in solid-liquid composite lubrication system. *Tribol Int* **161**: 107099 (2021)

[26] He B L, Liu S, Zhao X Y, Liu J X, Ye Q A, Liu S J, Liu W M. Dialkyl dithiophosphate-functionalized gallium-based liquid-metal nanodroplets as lubricant additives for antiwear and friction reduction. *ACS Appl Nano Mater* **3**(10): 10115–10122 (2020)

[27] Ye Q A, Liu S, Zhang J, Xu F, Zhou F, Liu W M. Superior lubricity and antiwear performances enabled by porous carbon nanospheres with different shell microstructures. *ACS Sustainable Chemistry & Engineering* **7**(14): 12527–12535 (2019)

[28] Li X L, Ling Y L, Zhang G L, Yin Y C, Dai Y J, Zhang C H, Luo J B. Preparation and tribological properties of solid-liquid synergetic self-lubricating PTFE/SiO_2/PAO6 composites. *Compos B* **196**: 108133 (2020)

[29] Song W, Yan J C, Ji H B. Tribological performance of an imidazolium ionic liquid-functionalized SiO_2@Graphene oxide as an additive. *ACS Appl Mater Interfaces* **13**(42): 50573–50583 (2021)

[30] Peng D X, Kang Y, Hwang R M, Shyr S S, Chang Y P. Tribological properties of diamond and SiO_2 nanoparticles added in paraffin. *Tribol Int* **42**(6): 911–917 (2009)

[31] Razavi S, Sabbaghi S, Rasouli K. Comparative investigation of the influence of $CaCO_3$ and SiO_2 nanoparticles on lithium-based grease: Physical, tribological, and rheological properties. *Inorg Chem Commun* **142**: 109601 (2022)

[32] Cui Y H, Xue S H, Wang S Y, Chen X, Liu S J, Ye Q A, Zhou F, Liu W M. Fabrication of carbon dots intercalated mxene hybrids via laser treatment as oil-based additives for synergistic lubrication. *SSRN Journal*: 373–382 (2022)

[33] Zhan Y J, Nan B F, Liu Y C, Jiao E X, Shi J, Lu M G, Wu K. Multifunctional cellulose-based fireproof thermal conductive nanocomposite films assembled by *in situ* grown SiO_2 nanoparticle onto MXene. *Chem Eng J* **421**: 129733 (2021)

[34] Du C F, Wang Z J, Wang X M, Zhao X Y, Gao J D, Xue Y Q, Jiang Y H, Yu H, Ye Q. Probing the lubricative behaviors of a high MXene-content epoxy-based composite under dry sliding. *Tribol Int* **165**: 107314 (2022)

[35] Cui Y H, Yang K, Wang J Q, Shah T, Zhang Q Y, Zhang B L. Preparation of pleated RGO/MXene/Fe_3O_4 microsphere and its absorption properties for electromagnetic wave. *Carbon* **172**: 1–14 (2021)

[36] Gong K L, Yin L, Shi C L, Qian X D, Zhou K Q. Dual char-forming strategy driven MXene-based fire-proofing epoxy resin coupled with good toughness. *J Colloid Interface Sci* **640**: 434–444 (2023)

[37] Hui X B, Zhao R Z, Zhang P, Li C X, Wang C X, Yin L W. Low-temperature reduction strategy synthesized Si/Ti_3C_2 MXene composite anodes for high-performance Li-ion batteries. *Adv Energy Mater* **9**(33): 1901065(2019)

[38] Wei H W, Dong J D, Fang X J, Zheng W H, Sun Y T, Qian Y, Jiang Z X, Huang Y D. $Ti_3C_2T_x$ MXene/polyaniline (PANI) sandwich intercalation structure composites constructed for microwave absorption. *Compos Sci Technol* **169**: 52–59 (2019)

[39] Zhang Y Y, Chen P, Wang Q Y, Wang Q A, Zhu K, Ye K, Wang G L, Cao D X, Yan J, Zhang Q A. High-capacity and kinetically accelerated lithium storage in MoO_3 enabled by oxygen vacancies and heterostructure. *Adv Energy Mater* **11**(31): 2101712 (2021)

[40] Li X L, Yin X W, Han M K, Song C Q, Xu H L, Hou Z X, Zhang L T, Cheng L F. Ti_3C_2MXenes modified with *in situ* grown carbon nanotubes for enhanced electromagnetic wave absorption properties. *J Mater Chem C* **5**(16): 4068–4074 (2017)

[41] Wang Y X, Lu Q, Xie H J, Liu S J, Ye Q, Zhou F, Liu W M. *In-situ* formation of nitrogen doped microporous carbon nanospheres derived from polystyrene as lubricant additives for anti-wear and friction reduction. *Friction* **12**(3): 439–451 (2024)

[42] Xie H J, Wang Y X, Wang P, Liu S J, Ye Q, Liu W M. Poly(tannic acid)-functionalized onion-like carbon nanoparticles derived from candle soot serving as potent lubricant additives. *J Mol Liq* **379**: 121697 (2023)

[43] Cui Y H, Xue S H, Chen X, Bai W, Liu S J, Ye Q, Zhou F. Fabrication of two-dimensional MXene nanosheets loading Cu nanoparticles as lubricant additives for friction and wear reduction. *Tribol Int* **176**: 107934 (2022)

[44] Tian P, Yu G M, Wei K X, Zhang Z X, Wang N. Effect of hydroxyl intercalation on tribological properties of MXene ($Ti_3C_2T_x$). *Ceram Int* **47**(21): 30722–30728 (2021)

[45] Wang P, Xie H J, Guo F Q, He B L, Wang X Z, Liu S J, Ye Q A, Liu W M. Thiadiazole dimer-functionalized liquid metal nanoparticles for anti-corrosion and friction reduction. *ACS Appl Nano Mater* **6**(7): 5799–5807 (2023)

Yuhong CUI. She received her bachelor degree from Taiyuan University of Technology in 2019 and her master degree from Northwestern Polytechnical University in 2022. She is currently a doctoral student in the Center of Advanced Lubrication and Seal Materials at School of Materials Science and Engineering, Northwestern Polytechnical University. Her research interest is MXene nanosheets as lubricant additives.

Qian YE. He is an associate professor at Northwestern Polytechnical University. He received his B.S. degree in Lanzhou University (2005), and got his Ph.D. degree in organic chemistry at Lanzhou University (2010). He spent one year (2013–2014) at Université catholique de Louvain as a research associate. His research interests focus on functional nanomaterials, surface modification, lubricant coating, and anti-fouling materials. His work has been published in more than 80 peer-reviewed papers with a current h-index of 32.

Feng ZHOU. He is a full professor in Lanzhou Institute of Chemical Physics, Chinese Academy of Sciences, China, and the director of State Key Laboratory of Solid Lubrication. He gained his Ph.D. degree in 2004 and spent three years (2005–2008) in the Department of Chemistry, University of Cambridge as a research associate. He has published more than 300 journal papers that received more than 25,000 citations and has the high-index of 88. His research interests include the bioinspired tribology, biomimic surfaces/ interfaces of soft matters, drag-reduction and antibiofouling, and functional coatings. He has gained a number of awards including "Outstanding Youth Award" of International Society of Bionic Engineering, 2013, and one National Award for Natural Sciences (the second class). He serves as an editorial board member of *Tribology International*, *Journal of Fiber Bioengineering and Informatics*, and *Friction*, etc.